Title

Coupled Thermo-Poro-Mechanical Finite Element Analysis of an Energy Foundation Centrifuge Experiment in Partially Saturated Silt

Authors

Wang, W
Regueiro, RA
McCartney, JS

Publication Date

2014-02-24

DOI

10.1061/9780784413272.258

Peer reviewed

Coupled Thermo-Poro-Mechanical Finite Element Analysis of an Energy Foundation Centrifuge Experiment in Partially Saturated Silt

W. Wang[1], R.A. Regueiro[1], J.S. McCartney[1]

[1]Department of Civil, Environmental, and Architectural Engineering
University of Colorado, Boulder, 428 UCB, Boulder, CO, 80309
wei.wang-2@colorado.edu, richard.regueiro@colorado.edu, john.mccartney@colorado.edu

ABSTRACT: This paper presents an axisymmetric fully coupled thermo-poro-mechanical (TPM) finite element analysis (FEA) of a single energy foundation centrifuge experiment in partially saturated silt conducted at the University of Colorado, Boulder (UCB). The motivation is to explore thermo-mechanical effects on the foundation performance, and thermally-induced liquid and gas flow inside the surrounding soil. The paper compares modeling outcomes and experimental observations regarding thermal strains and displacements of foundations due to heating. The coupled FE model predicts solid skeleton deformation, suction, and volumetric water contents of the soil, and analyzes the thermally-induced pore water vapor flow and liquid water flow.

1 Introduction

Energy foundations have become more popular as an energy-saving and environmentally-friendly technology, compared with traditional energy systems. With adequate design and installation, energy foundations can fulfill not only the geotechnical but also the thermal requirements of buildings without relying solely on conventional heating and cooling systems. Relevant investigations and studies in the past decade have indicated the feasibility of this innovative technology both technically and economically (Hepbasli, 2003; Laloui et al., 2006).

A number of constitutive models have been developed to study the heat and mass transport problem in rigid porous media (Milly, 1982; Bear et al., 1991). Gawin et al. (1995); Thomas and Missoum (1999) considered the deformation of soil solid skeleton to enhance the coupled thermo-poro-mechanical effects by coupling elasticity theory with the state surface approach. Khalili and Loret (2001) proposed elasto-plastic models to account for the nonlinear deformation behavior of solid skeleton and the variation of the yield surface with temperature and suction. Many attempts have been made to explore thermal effects on hydro-mechanical behavior of partially saturated soils experimentally (Romero et al., 2001; Wu et al., 2004).

Although some construction observations and relevant studies have been conducted, further research regarding geotechnical and thermal issues is still necessary in order to investigate the complex interactions among temperature change, induced effective stress, and pore fluid flow in partially saturated soils, and also to provide guidance for the design and installation of energy foundations. For example, thermal expansion and contraction of foundations together with thermally-induced consolidation of soil may

lead to the loss of soil-foundation side shear resistance, thus affecting the mechanical response of energy foundations and their structural performance.

This paper employs an axisymmetric fully coupled TPM finite element (FE) model to simulate soil-structure interaction (SSI) in partially saturated silt for a centrifuge energy foundation experiment conducted at the University of Colorado, Boulder (UCB). We present briefly the governing equations and implementation of a fully coupled thermo-poro-elastic FE model. In this model, partially saturated soil is treated as a three-phase mixture (solid, liquid and gas) or four constituent mixture (solid, liquid water, water vapor and dry air). The gas phase is considered to be a combination of dry air and water vapor. The model is implemented for small strain analysis. Nodes of the energy foundation and soil meshes at the interface are assumed to have no relative displacement in this implementation (rigid connection), but this assumption will be relaxed in future work when considering a TPM interface element.

Notation: Bold-face letters denote matrices, tensors and vectors. Cylindrical coordinates are employed, with the vector of coordinates $\boldsymbol{r} = [r, z]$. Solid mechanics sign convention is used, i.e., $\sigma > 0$ and $\varepsilon > 0$ for tension; $\sigma < 0$ and $\varepsilon < 0$ for compression.

2 Couple Finite Element Formulation

The governing equations are developed based on the mixture theory of porous media, and satisfy the balance of mass, linear momentum and energy conservation, as well as reduced dissipation inequality derived from the second law of thermodynamics (de Boer, 2005). Solid and liquid water are assumed to be isotropic and mechanically-incompressible, yet the soil solid skeleton is compressible; individual constituents can thermally expand or contract. With details omitted, Table 1 briefly summarizes the governing equations and constitutive equations adopted in the model. The field variables are soil solid-skeleton displacement $\boldsymbol{u}$, pore water pressure p_w, pore gas pressure p_g and soil mixture temperature θ.

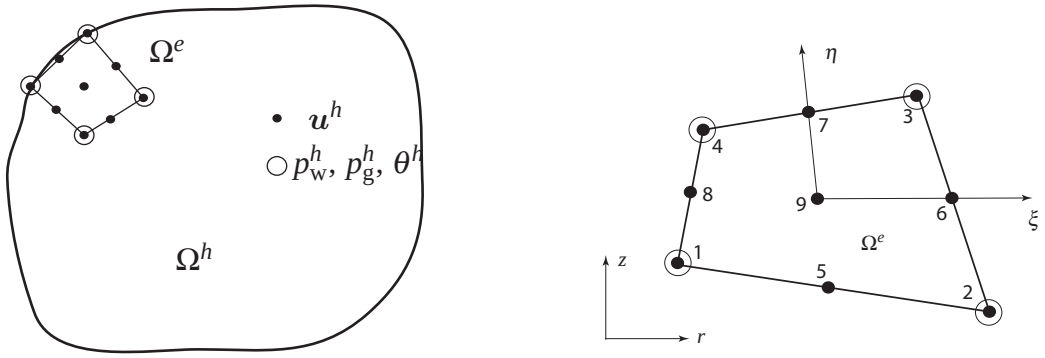

FIG. 1. Discretization into mixed quadrilateral elements.

A weighted residual method is used to formulate the coupled variational equations from the coupled governing differential equations, which are then discretized using

finite elements. Quadrilateral finite elements with biquadratic interpolation in solid-skeleton displacement, bilinear in pore water pressure, pore gas pressure and soil mixture temperature are employed to ensure numerical stability (see Fig. 1). Details aside, we arrive at a coupled nonlinear first order ordinary differential equation to solve, using generalized trapezoidal rule for time integration, and Newton-Raphson nonlinear algorithm.

3 Numerical Example

A simplified axisymmetric FE mesh containing 30 elements (Fig. 2) is created to simulate SSI of an end-bearing energy foundation under thermal, hydraulic, and mechanical loads in the centrifuge experiment with centrifugation to an acceleration of 24 times gravity. In the experiment, the foundation is heated in stages over a range of temperatures expected in the field through P4-P7 as shown in Fig. 3. The partially saturated soil is modeled as an overconsolidated soil layer with linear thermo-elastic behavior. Elastic, hydraulic, and thermal parameters are applied for Bonny silt. Fluid

Table 1. Governing equations and constitutive equations

Governing equations	
Balance of linear momentum of mixture:	$\nabla\boldsymbol{\sigma} + \rho\boldsymbol{b} = \mathbf{0}$
Balance of mass for water species (liquid water and water vapor):	$(\rho^{wR}S_w + \rho^{gvR}S_g)\mathrm{div}\,\boldsymbol{v}_s + n(\rho^{wR} - \rho^{gvR})\frac{D^sS_w}{Dt} - \left[(1-n)(\rho^{wR}S_w + \rho^{gvR}S_g)\beta_s^\theta + n\rho^{wR}S_w\beta_w^\theta\right]\frac{D^s\theta}{Dt} + nS_g\frac{D^s\rho^{gvR}}{Dt} + \mathrm{div}(\rho^{gvR}\,\tilde{\boldsymbol{v}}_{gv}^s + \rho^{wR}\,\tilde{\boldsymbol{v}}_w^s) = 0$
Balance of mass for dry air:	$\rho^{gaR}S_g\mathrm{div}\,\boldsymbol{v}_s - \rho^{gaR}S_g\beta_s^\theta(1-n)\frac{D^s\theta}{Dt} + nS_g\frac{D^s\rho^{gaR}}{Dt} - n\rho^{gaR}\frac{D^sS_w}{Dt} + \mathrm{div}(\rho^{gaR}\,\tilde{\boldsymbol{v}}_{ga}^s) = 0$
Energy conservation of mixture:	$(\rho C)_m\frac{D^s\theta}{Dt} + \rho^{wR}C^w\,\tilde{\boldsymbol{v}}_w^s\cdot\mathrm{grad}\,\theta + \rho^{gR}C^g\,\tilde{\boldsymbol{v}}_g^s\cdot\mathrm{grad}\,\theta - \rho r + \mathrm{div}\,\boldsymbol{q} + \hat{\rho}^{gv}H_{vap} = 0$
Constitutive equations	
Velocity of liquid water $(k=w)$ or gas mixture $(k=g)$ (Darcy's law):	$\widetilde{\boldsymbol{v}}_k^s = -\frac{\kappa(n)K_{rk}(S_w)}{\mu_k(\theta)}(\nabla p_k - \rho^{kR}\boldsymbol{g})$
Velocity of vapor $(k=gv)$ or dry air $(k=ga)$ (Darcy's law and Fick's law):	$\widetilde{\boldsymbol{v}}_k^s = nS_g\widetilde{\boldsymbol{v}}_k = -\frac{\kappa(n)K_{rg}}{\mu_g(\theta)}\nabla p_g - D\,\nabla\left[\ln\left(\frac{p_k}{p_g}\right)\right]$
Ideal gas law:	$\rho^{gv} = p_{gv}M_w/\theta R;\quad \rho^{ga} = p_{ga}M_a/\theta R$
Dalton's law:	$\rho^g = \rho^{gv} + \rho^{ga};\quad p_g = p_{gv} + p_{ga}$
Kelvin's law:	$\mathrm{RH} = p_{gv}/p_{gvs}(\theta) = \exp\left(-sM_w/R\theta\rho^{wR}\right)$
Fourier's law:	$\boldsymbol{q} = -\boldsymbol{K}_{eff}^\theta\nabla\theta$

parameters are assumed for water. The geometry of the FE model is the same as that in the experiments. The height of the energy foundation is $H = 0.537m$. The radius of the energy foundation is $a = 0.025m$, and the radius of the centrifuge bucket is $R = 0.3025m$.

Initial conditions and boundary conditions are simplified according to knowledge of the experimental conditions. The initial conditions include: porosity $n_0 = 0.425$; volumetric water content $w_0 = 26\%$; suction $s_0 = 32kPa$; gas pressure $p_{g0} = 101kPa$; temperature $\theta_0 = 20^oC$. As for boundary conditions, due to the axisymmetry of the problem, and assumed rigidity of the bucket, nodal displacements on the z axis ($r = 0$) and right edge ($r = R$) are $u_r = 0$, and nodal displacements on the bottom ($z = -H$) are $u_z = 0$. An unreinforced concrete energy foundation is assumed to be impermeable in

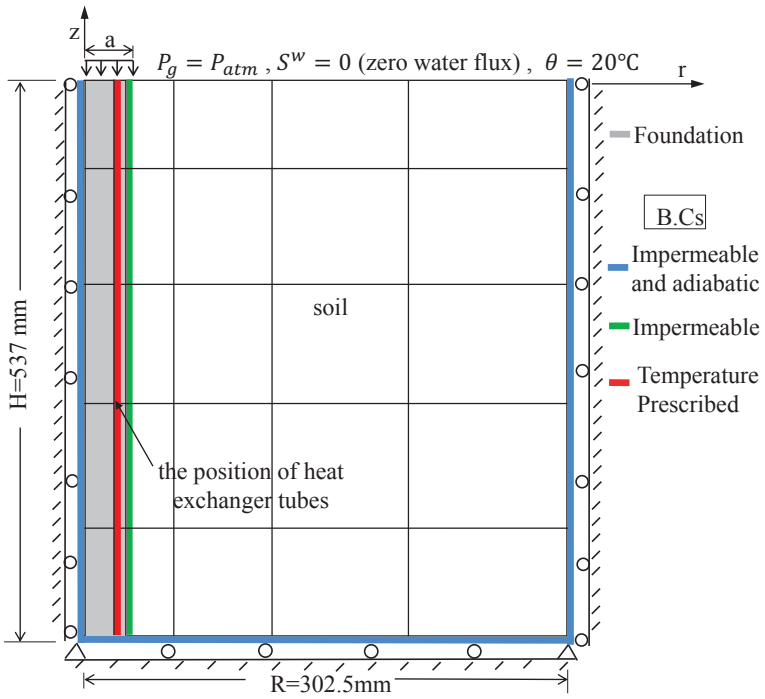

FIG. 2. Axisymmetric FE mesh and geometry for simulating end-bearing energy foundation centrifuge experiment. Boundary conditions are included.

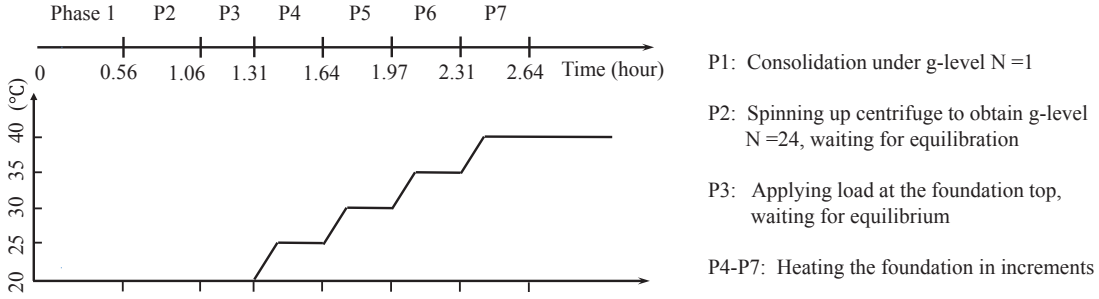

FIG. 3. Schematic of testing procedure for energy foundation centrifuge experiment (P:Phase).

this analysis. Also zero water flux $S^w = 0$ at the top of soil is assumed. The pore gas pressure p_g on the top is held to be atmospheric pressure p_{atm}. In the experiment or the field, the temperature of the energy foundation is actually controlled by circulating fluid with a known temperature through a series of three equally spaced "U" shape heat exchanger tubes attached to the inside of the reinforcement cage at $r = 0.02m$. Technically, a 3-D model including a CFD analysis of the heated fluid flow through the tubes would be a more accurate estimate of the thermal boundary condition. However, for simplicity, we assume that temperature is prescribed along the z axis at $r = 0.02m$. During circulation of heated fluid through the heat exchange elements in the foundation, energy foundations typically reach a relatively constant temperature with depth. This has been observed in several previous laboratory studies (Stewart and McCartney, 2013). The constant temperature conditions were selected in the study to evaluate the thermo-mechanical soil-structure interaction behavior of the foundation, not to evaluate the transient heat transfer processes, which we agree would be better simulated with a heat flux boundary condition. The temperature at the top of the soil is held constant at room temperature (20 °C), and the other surfaces are adiabatic as indicated in Fig. 2. Axial load is exerted on the top of the energy foundation instantaneously, and is kept constant during the test. Effective solid-skeleton traction $\boldsymbol{t}^{\sigma'} = [0 \ -t^{\sigma'}]$, $t^{\sigma'} = 384kPa$, is applied on the top of the energy foundation. The parameters of the unreinforced concrete energy foundation (c) and soil (Table 2) are determined from experimental measurements and other references (Stewart and McCartney, 2013).

Table 2. Parameters used in the FEA.

Parameter	Symbol	Value	Unit
Linear thermal expansion coefficient of concrete	β_c^θ	7.5×10^{-6}	$/K$
Linear thermal expansion coefficient of solid skeleton	β_{skel}^θ	8.7×10^{-6}	$/K$
Linear thermal expansion coefficient of soil solid	β_s^θ	1.17×10^{-5}	$/K$
Specific heat capacity of concrete	C_c	855	$J/(K \cdot kg)$
Specific heat capacity of soil solid	C_s	1000	$J/(K \cdot kg)$
Specific gravity of soil solid	G_s	2.6	
Thermal conductivity of concrete	K_c^θ	2.6	$W/(m \cdot K)$
Thermal conductivity of solid	K_s^θ	1.24	$W/(m \cdot K)$
Young's modulus of concrete foundation	E_c	7.17×10^9	Pa
Poisson's ratio of concrete foundation	ν_c	0.18	m/m
Lam*é* parameter of soil solid skeleton	λ_{skel}	2.9×10^7	Pa
Lam*é* parameter of soil solid skeleton	μ_{skel}	4.7×10^7	Pa
van Genutchen model parameter	α	0.357×10^{-4}	Pa^{-1}
van Genutchen model parameter	n	1.8	
Hydraulic conductivity of saturated soil	k_{sat}	1.3×10^{-7}	m/s

4 Results

Fig. 4 - Fig. 15 are plotted contours of various results on the deformed mesh with

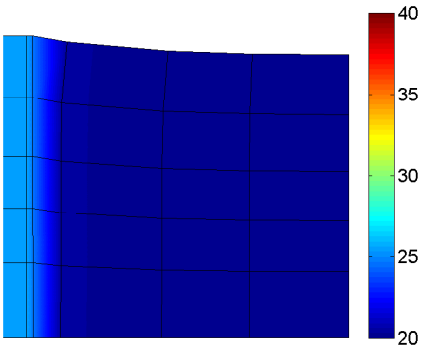

FIG. 4. Temperature (^oC) contour at $\Delta\theta = 5^oC$ (the end of phase 4).

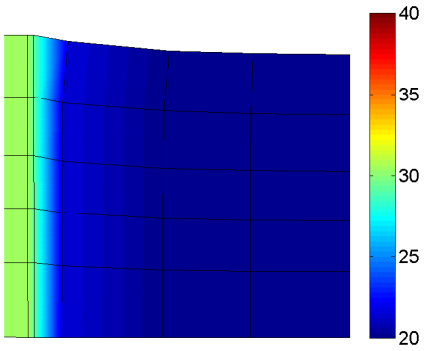

FIG. 5. Temperature (^oC) contour at $\Delta\theta = 10^oC$ (the end of phase 5).

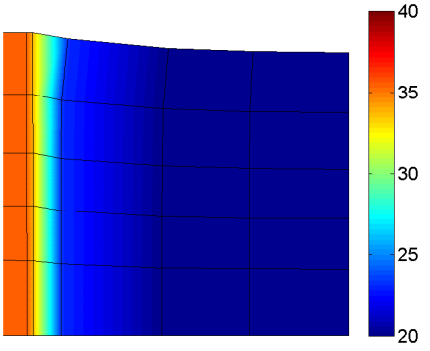

FIG. 6. Temperature (^oC) contour at $\Delta\theta = 15^oC$ (the end of phase 6).

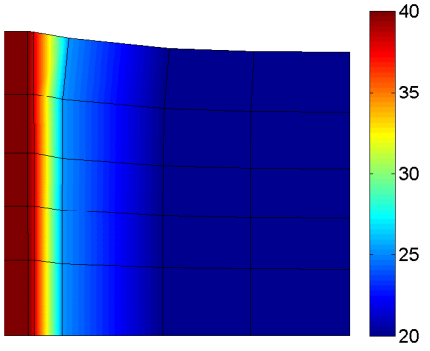

FIG. 7. Temperature (^oC) contour at $\Delta\theta = 20^oC$ (the end of phase 7).

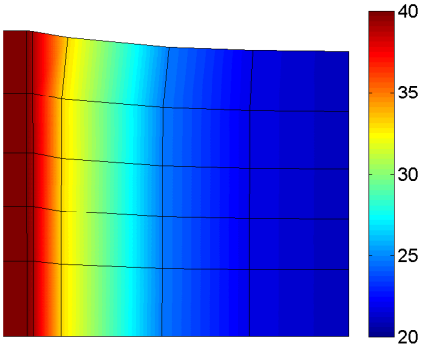

FIG. 8. Temperature (^oC) contour at 10 hours after the last thermal loading phase.

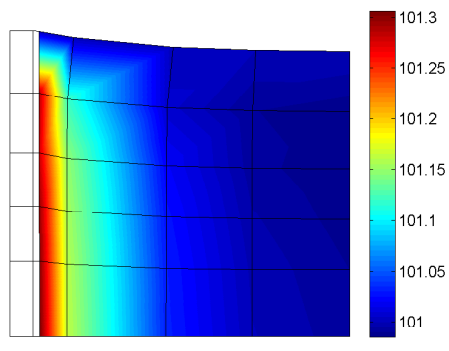

FIG. 9. Contour of pore gas pressure (kPa) in soil at 10 hours after the last thermal loading phase.

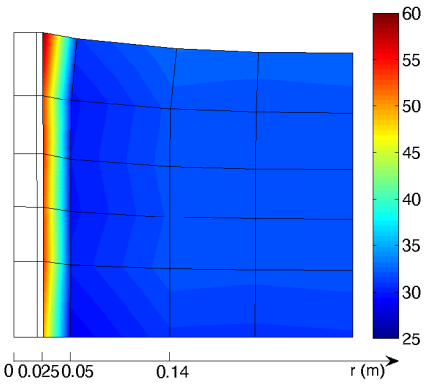

FIG. 10. Contour of suction (kPa) in soil at 10 hours after the last thermal loading phase.

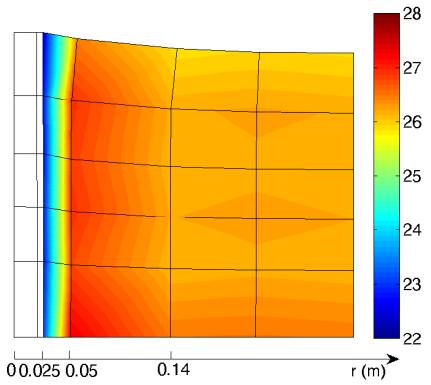

FIG. 11. Volumetric water content (%) contour in soil at 10 hours after the last thermal loading phase.

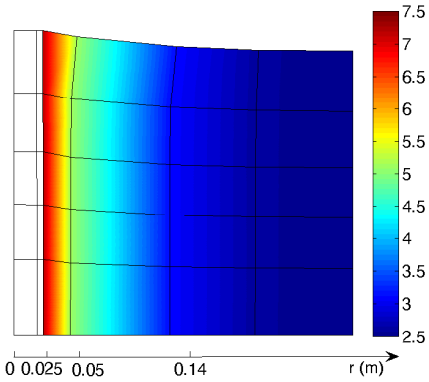

FIG. 12. Contour of pore water vapor pressure (kPa) in soil at 10 hours after the last thermal loading phase hours.

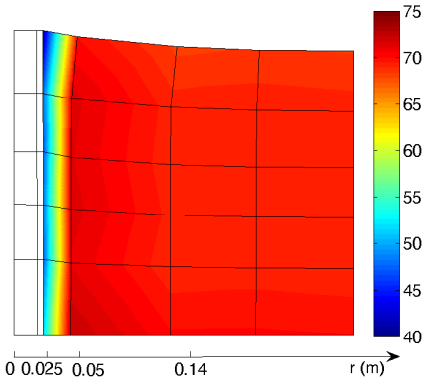

FIG. 13. Contour of pore water pressure (kPa) in soil at 10 hours after the last thermal loading phase.

displacement magnification factor equal to 100. Temperature contours (Fig. 4 - Fig. 7) indicate that although the foundation reaches steady temperatures after each stage, the soil is not necessarily at steady-state temperature, for example, soil mixture temperature remains near the initial value $\theta_0 = 20^oC$ at further radial distance in the soil. This means that the system response is representative of transient heating. About 10 hours after the end of phase 7 (phase 7 ends at about 2.64 hr), higher temperature is observed inside the soil near the foundation, as shown in Fig. 8. Variation of the pore gas pressure is negligible during the heating process as shown in Fig. 9. Fig. 10 and Fig. 11 indicate significant changes in suction and volumetric water content respectively near the soil-foundation interface. For example, suction increases from an initial value of $32kPa$ to nearly $60kPa$ near the interface ($r = 0.025m$), and smaller rise occurs in the soil at $r = 0.05m$. Suction drops slightly in the region of $0.05m < r < 0.14m$, however, no significant variation of suction is observed beyond $r = 0.14m$. A corresponding trend

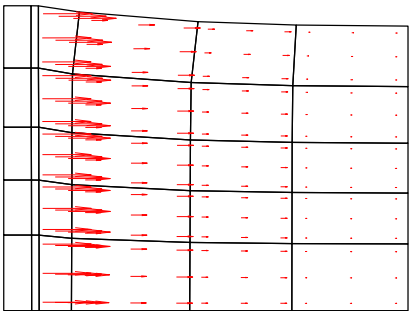

FIG. 14. Pore water vapor flow vectors in soil at 10 hours after the last thermal loading phase.

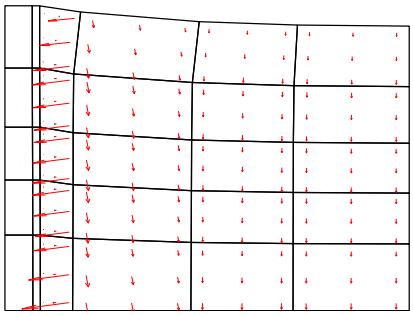

FIG. 15. Pore water flow vectors in soil at 10 hours after the last thermal loading phase.

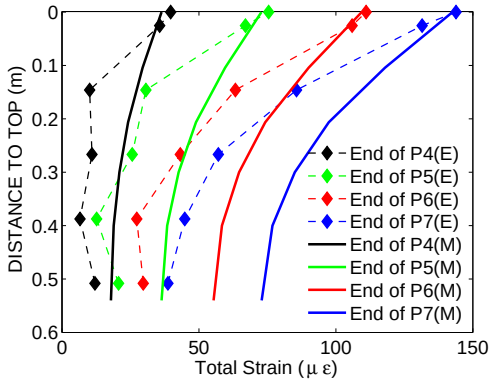

FIG. 16. Comparison of total vertical strain ε_{zz} between experimental (E) data and model (M) predictions inside the energy foundation.

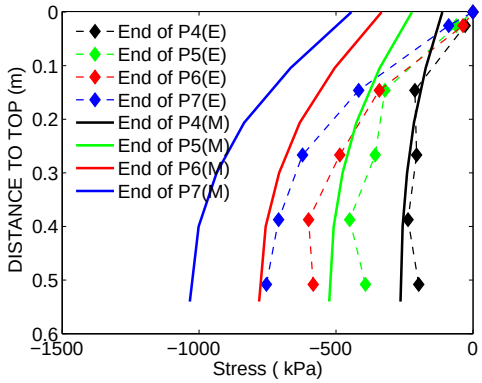

FIG. 17. Comparison of stress σ_{zz} between experimental (E) calculations and model (M) predictions inside the energy foundation.

is detected regarding volumetric water content distribution. Fig. 12 indicates that a net rate of evaporation is produced within the soil due to rapidly increasing temperatures. A sharp rise of water vapor pressure (from initial value of $2.5kPa$ to around $7kPa$) happens near the soil-foundation interface ($r = 0.025m$), and a smaller rise occurs further from the interface. The formed density gradients drive vapor from the hotter region (soil-foundation interface) to the cooler region. Arrows in Fig. 14 show the direction of water vapor flow inside the soil. Also, higher vapor velocity is observed under larger temperature gradients. This diffusion process is governed by many factors including hydraulic and thermal properties of soil, which require further research. Condensation occurs when the hotter vapor migrates to the region of lower temperature, and hence leads to a rise in volumetric water content, as shown in Fig. 11 at $0.05m < r < 0.14m$. As the soil near the soil-foundation interface becomes drier ($p_w \approx 45kPa$ at $r = 0.025m$) compared to the soil further from the interface ($p_w \approx 70kPa$ at $r = 0.05m$), pore water pressure gradients are formed ,which force liquid water to flow from the wetter region

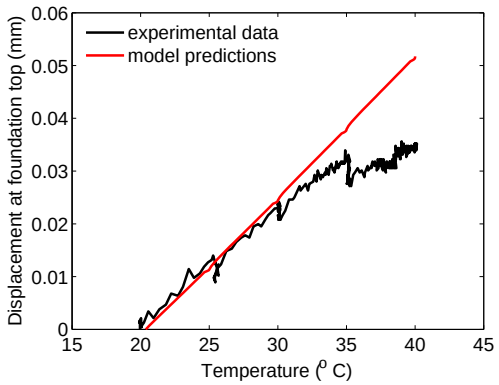

FIG. 18. Plot of vertical displacement versus temperature at the center of the foundation top.

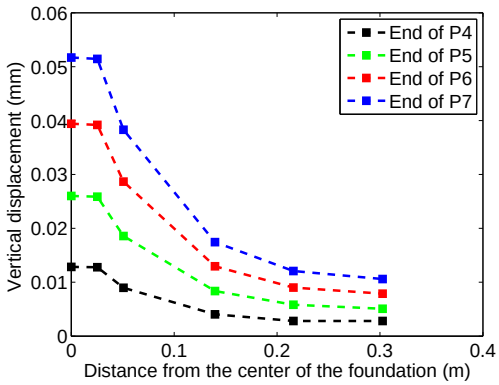

FIG. 19. Vertical displacement d_z of the top of the energy foundation and soil surface as a function of r at different Phases.

to the drier region, as shown in Fig. 13. The movement of pore water is illustrated by the direction of water flow inside the soil in Fig. 15. In the soil at further radial distance, gravity mainly induces downward pore water flow. The pore liquid water flow is in the direction of the soil-foundation interface near the interface. The comparison of thermal strain between FEA and experimental results in Fig. 16 shows good agreement at the foundation top, with similar trend observed for the rest of the foundation. One of the possible reasons for the difference is the assumption of perfect bond at the soil-foundation interface in the model, therefore, side shear resistance along the length of the foundation is not well represented. Implementation of interface elements at the soil-foundation interface will allow closer representation of the SSI conditions. Fig. 17 indicates that both experimental and modeling results show smaller thermally induced stress at the top of the foundation. Fig. 18 shows good agreement of displacement at the foundation top in the temperature range of $20^oC - 30^oC$, but in the range $30^oC - 40^oC$, the linear elastic solid skeleton constitutive behavior and function of temperature needs to be modified. The thermal expansion coefficient of the energy foundation estimated from Fig. 18 is $\approx 6.8 \times 10^{-6}/K$. This value is slightly smaller than the given parameter $\beta_c^\theta = 7.5 \times 10^{-6}/K$ due to the assumption of perfect bond at the soil-foundation interface in the FEA model. This assumption will be relaxed when the interface element is implemented. The top displacements of foundation and soil are shown in Fig. 19 with respect to radial coordinate r and Phase loading. The deformation of soil is a combination of thermal expansion and solid skeleton consolidation due to gravity level increases in centrifuge experiments.

5 Conclusions

This paper applies a fully coupled thermo-poro-mechanical (TPM) FE model of partially saturated, linear isotropic elastic soil solid skeleton to simulate change of temperature, displacement, and strain in an energy foundation as well as suction and volumetric water contents in the soil through SSI. One issue is the identification of the thermal boundary conditions. For example, the top ($z = 0$) temperature is simply as-

sumed to be constant (room temperature). This boundary condition could be improved by considering evaporation fluxes at the top of soil due to soil-atmosphere interaction. Also, the assumption of prescribed temperature along the direction z at $r = 0.02m$ in the model does not represent the experimental condition exactly. Extension of the axisymmetric model to 3D and inclusion of a CFD analysis could resolve this issue. In addition, implementation of interface elements at the soil-foundation interface will allow us to better represent the interaction between soil and pile.

Acknowledgements

Funding for this research was provided by National Science Foundation grant CMMI-0928159. This funding is gratefully acknowledged.

References

Bear, J., Bensabat, J., and Nir, A. (1991). "Heat and mass transfer in unsaturated porous media at a hot boundary. i. one-dimensional analytical model." *Transport in Porous Media*, 6(3), 281 – 298.

de Boer, R. (2005). *Trends in continuum mechanics of porous media*, Vol. 18. Springer.

Gawin, D., Baggio, P., and Schrefler, B. A. (1995). "Coupled heat, water and gas flow in deformable porous media." *International Journal for numerical methods in fluids*, 20(8-9), 969–987.

Hepbasli, A. (2003). "Current status of geothermal energy applications in Turkey." *Energy Sources*, 25(7), 667 – 77.

Khalili, N. and Loret, B. (2001). "An elasto-plastic model for non-isothermal analysis of flow and deformation in unsaturated porous media: formulation." *International Journal of Solids and Structures*, 38(46-47), 8305 – 30.

Laloui, L., Nuth, M., and Vulliet, L. (2006). "Experimental and numerical investigations of the behaviour of a heat exchanger pile." *International Journal for Numerical and Analytical Methods in Geomechanics*, 30(8), 763–781.

Milly, P. (1982). "Moisture and heat transport in hysteretic, inhomogeneous porous media: a matrix head-based formulation and a numerical model." *Water Resources Research*, 18(3), 489 – 98.

Romero, E., Gens, A., and Lloret, A. (2001). "Temperature effects on the hydraulic behaviour of an unsaturated clay." *Geotechnical and Geological Engineering*, 19(3-4), 311 – 332.

Stewart, M. A. and McCartney, J. S. (2013). "Centrifuge modeling of soil-structure interaction in energy foundations." *ASCE Journal of Geotechnical and Geoenvironmental Engineering*, in press.

Thomas, H. and Missoum, H. (1999). "Three-dimensional coupled heat, moisture, and air transfer in a deformable unsaturated soil." *International Journal for Numerical Methods in Engineering*, 44(7), 919 – 43.

Wu, W., Li, X., Charlier, R., and Collin, F. (2004). "A thermo-hydro-mechanical constitutive model and its numerical modelling for unsaturated soils." *Computers and Geotechnics*, 31(2), 155 – 167.